Geochemistry of dissolved carbon in pelagic and benthic ecosystems

G. Crispi
Istituto Nazionale di Oceanografia e di Geofisica Sperimentale - OGS
June 2023, 57 pp., Trieste

1. Introduction

Integrated modeling of relevant processes helps in the treatment of impacts on aquatic and marine sedimentary systems, including both potential changes due to CO_2 and CH_4 emissions of natural and anthropogenic origin, and ecosystem risks deriving from gas leaks in geological storage.

The main objective of this work is to evaluate the CO_2 and CH_4 fluxes, which depend on salinity, sea temperature and total alkalinity, dissolved inorganic carbon and nutrient concentration, sea state, wind speed, kinematic viscosity, solubility and diffusion of CO_2, partial pressure of CO_2 in the atmosphere and Bunsen coefficient of methane (Wanninkhof, 1992). The marine description combines the interactions between components of several sub-models: pelagic, boundary layer, benthic sedimentary and biological systems.

Preliminary models of the Mediterranean ecosystem have been used to simulate bacterial growth rates and dynamics (Vichi et al., 2003) and to assimilate biomass into operational schemes (Crispi et al., 2006). The carbon cycle and parameterization of related processes have been achieved by defining the behavior and variability of total alkalinity throughout the water column (Peng et al., 1987). This approach requires the definition of the contributions to alkalinity of water dissociation in seawater and of nutrients: dissolved inorganic carbon, phosphates, silicates, nitrates, nitrites and ammonia (Galloway et al., 2004).

The marine cycle of sulphur changes and, in turn, is affected by the total alkalinity of the sea. For example, reducing one mole of sulphate increases total alkalinity by two mole equivalents. The estimate of the sulphate, given the geochemical abundance of hydrofluoric acid, an ion in solution of hydrogen fluoride, can be taken into consideration knowing the pH and the activity of the hydrogen ion. Therefore, a thorough modeling allows the evaluation of both sulphate reduction and sulphate concentration, to give adequate boundary conditions to the upper sedimentary layer (Gaidos, et al. 2007).

Sedimentary processes are followed in their evolution by first stage schemes of benthic diagenesis outlined by Boudreau (1996) in the general case and applied by Luff and Moll (2004) in the North Sea introducing total carbonate and calcite dynamics.

Other ecological applications to benthos modelling have also been designed in the MAST frame of the European Regional Seas Ecosystem Model: nutrient cycling

(Ruardij and Van Raaphorst, 1995) in the northern and southern North Sea, benthic processes (Ebenhöh et al., 1995) in the Wadden Sea inside the ICES box 8, and microphytobenthos (Blackford, 2002) in the northern Adriatic Sea.

The former applications use constant gradient boundary condition at the sediment bottom and the latter use constant concentration boundary conditions.

In the present work, the evaluation of CO_2 and CH_4 emission rates from the seabed is assisted by the mass content in the benthos, taking into account the cycling of inorganic nutrients in the oxygenated and reducing layers of the sediment, with the anoxic layer separated from the reducing one. The CO_2-Geo numerical model is set up using Dirichlet boundary conditions at the sediment-sea interface and Neumann boundary conditions at the base of the sedimentary system, where CO_2 and CH_4 losses can occur.

The reason for using these study environments lies in the objective of this work which consists in preparing an accurate and efficient mathematical tool from a computational point of view on an average scale from a few weeks to a few years. The possibility then of using this method even over long periods, from a few years to a few decades, lies in the lack or negligibility of deviations from the averages of the ecosystem sizes, a point which is considered in the second paragraph. Also, some possible options are covered in Plate 1.

CO_2-Geo manages methanogenesis and methanotrophy and changes in CO_2 and CH_4 concentrations of the lower anoxic layer, increasing the production of methane in the sediment; the latter is present in the intermediate reducing layer and produces carbonates

and hydrogen sulphide (Boetius et al., 2000). Excess H_2S can be neutralized by sulphur reduction reactions, microbiologically mediated, or precipitated as pyrite when iron is available. The oxidation of methane takes place in the upper oxygenated layer. In the next section the complete method of sediment description is described: first in two cases used in sensitivity and precision applications; then in the general solution given respectively in the text and in the appendix; finally, in the benthic solver used to describe the short- and medium-term evolution.

2. Materials and Methods

2.1 Single-Layer Treatment

We begin with examples of single layers: L thick, ϕ porosity, D diffusion constant.

The diffusion equation of the concentration C(z,t) in the layer is

$$\frac{\partial C}{\partial t} = D\frac{\partial^2 C}{\partial z^2}$$

In the first example with no zero-order sources or sinks and flux *F* at z=L, the solution is

$$C(z,t) = \frac{Fz}{\phi D} + \frac{\pi FL}{4\phi D} e^{-D\pi^2 t/4L^2} \sin\frac{\pi z}{2L}$$

with the average concentration in the layer varying from the initial value <C(z,0)>=FL/D to the asymptote <$\underline{C}$(z)>=FL/2D for t→∞. The boundary conditions are: Dirichlet at the first extremal, $C(z=0,t)=0$, Neumann at the second extremal,

$$\frac{\partial C(z=L,t)}{\partial z} = \frac{F}{\phi D}.$$

The time derivative of the concentration results

$$\frac{\partial C(z,t)}{\partial t} = -\frac{F\pi^3}{16\phi L} e^{-D\pi^2 t/4L^2} \sin\frac{\pi z}{2L}$$

giving the following increase of the concentration

$$\Delta C(z,t) = C(z,t+\Delta t) - C(z,t) =$$
$$= \Delta t \frac{Fz}{\phi D}\frac{D\pi^2}{4L^2} - \Delta t \frac{D\pi^2}{4L^2}\left(\frac{Fz}{\phi D} + \frac{F\pi L}{4\phi D} e^{-D\pi^2 t/4L^2} \sin\frac{\pi z}{2L}\right) =$$
$$= \Delta t \frac{D\pi^2}{4L^2}[\underline{C}(z) - C(z,t)]$$

For what regards the increase of the average concentration in the layer, ΔC, we obtain the compact expression

$$\Delta < C(z,t) >= \Delta\left[\int_0^L dz C(z,t)\right] = \Delta t \frac{D\pi^2}{4L^2}[< \underline{C}(z) > - < C(z,t) >]$$

The total flux $F_{IN}(t)$ toward the environment, i.e. at the sediment-sea interface z=0, is

$$F_{IN}(t) = \frac{F}{\phi D} + \frac{F\pi^2}{8\phi D} e^{-D\pi^2 t/4L^2}$$

In the second example we consider the evolution of the concentration

$$C(z,t) = C(z = L/2)e^{-D\pi^2 t/L^2} \sin\frac{\pi z}{L}$$

C(0,t)=0, C(L,t)=0, and the flux at z=L is null (Carslaw and Jaeger, 1959). In this case

$$\Delta C(z,t) = -\Delta t C(z = L/2, t = 0)\frac{D\pi^2}{L^2}e^{-D\pi^2 t/L^2} \sin\frac{\pi z}{L} = \Delta t \frac{D\pi^2}{L^2}[\underline{C}(z) - C(z,t)]$$

and the final expression is as compact as the solution of the first example, i.e. with Neumann condition at the sediment bottom and Dirichlet condition at sediment-sea interface; the rates toward the asymptote are four times those of the first example.

Averaging along the layer, we obtain the variation of the concentration

$$\Delta C = \Delta t \frac{D\pi^2}{L^2}[< \underline{C}(z) > - < C(z,t) >]$$

In this case the flux toward the aquatic environment is

$$F_{IN}(t) = C(z = L/2, t = 0)\frac{\pi}{L}e^{-D\pi^2 t/L^2}$$

with an equal and opposite flux toward the deep sediment.

2.2 Environmental Fluxes

The general solution in the case of leakage from the bottom of the ecosystem is calculated, analogously to the first 2.1 example, expanding in sine series of sin(β_nL), with 2/L norm and eigenvalues given by cos(β_nL)=0, i.e. $\beta_n L=\pi/2+(n-1)\pi$ or $\beta_n L=(2n-1)\pi/2$

$$C(z,t)=\sum_{n=1}^{\infty} C_n(t)\sin\frac{(2n-1)\pi z}{2L}$$

The Fourier coefficients are

$$C_n(t)=\frac{2}{L}\int_0^L dz C(z,t)\sin\frac{(2n-1)\pi z}{2L}$$

The results of the integration for the second derivative with indices n=1,2,3, …

$$\frac{2}{L}\int_0^L dz\frac{\partial^2 C(z,t)}{\partial z^2}\sin\frac{(2n-1)\pi z}{2L}=(-1)^{n+1}\frac{2P_B(t)}{\phi DL}+\frac{(2n-1)\pi A(t)}{L^2}-\frac{(2n-1)^2\pi^2}{4L^2}C_n(t)$$

and extremal conditions $C(z=0,t)=A(t)$ and $\partial C/\partial z\big|_{z=L}=P_B(t)/\phi D$; the initial condition is $C(z,t=0)=\psi(z)$ and the coefficients of the initial conditions are given by

$$\psi_n = \frac{2}{L}\int_0^L dz\,\psi(z)\sin\frac{(2n-1)\pi z}{2L}$$

The equation to be solved, considering a homogeneous internal source, S(t)/L, sum of all the sources and sinks in the layer, is

$$C_n'(t) = (-1)^{n+1}\frac{2P_B(t)}{\phi L} + \frac{(2n-1)\pi DA(t)}{L^2} - \frac{(2n-1)^2\pi^2 D}{4L^2}C_n(t) + \frac{4S(t)}{(2n-1)\pi L}$$

Integrating and grouping the terms the solution results

$$C_n(t) = \psi_n e^{-(2n-1)^2\pi^2 Dt/4L^2} + \int_0^t d\tau e^{-(2n-1)^2\pi^2 Dt/4L^2}\left\{(-1)^{n+1}\frac{2P_B(\tau)}{\phi L} + \frac{(2n-1)\pi DA(\tau)}{L^2} + \frac{4S(\tau)}{(2n-1)\pi L}\right\}$$

On the other hand, the problem of Dirichlet (Amerio, 1976) for the second 2.1 example, with time-variable boundary conditions C(0,t)=A(t) and C(L,t)=B(t), is analysed for general environmental conditions and porosity Φ in the appendix.

2.3 Three-Layer Treatment

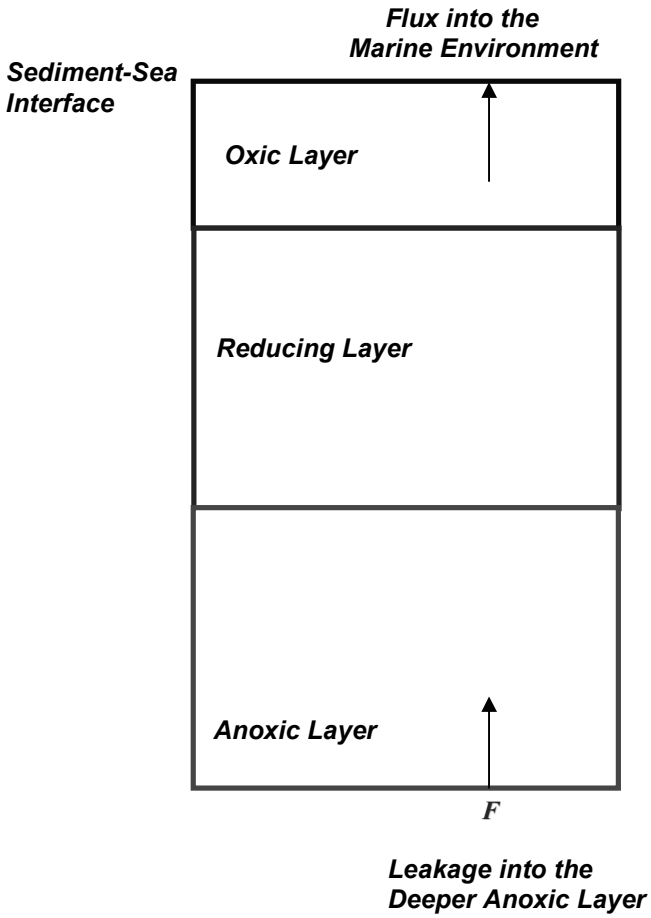

Fig. 1. Vertical geometry of the three layers.

In the upper layer the boundary condition between seawater and porewater is $C(z_0=0,t)=C_0$ and the boundary value C_1 between the upper and middle layer results

$$C(z_1 = L_1, t) = C_1 = C_0 + \left(\frac{S_1}{2} + \sum_{i=2}^{n} S_i + F \right) \frac{z_0 - z_1}{D_1}$$

where n is the number of layers in the sediment, n=3 in our case; F is flux applied to the bottom of the benthic ecosystem at depth L_3.

The respective average asymptotic concentration is

$$\underline{C}_1 = C_0 + \left(\frac{S_1}{3} + \frac{\sum_{i=2}^{n} S_i}{2} + \frac{F}{2} \right) \frac{z_0 - z_1}{D_1}$$

and give consistently the increase of the variable $C_1(z,t)$ averaged along the layer, from time t to time t+Δt

$$\Delta < C_1(z,t) >= \frac{\Delta t \pi^2 D_1}{4(z_0 - z_1)^2} (< \underline{C}_1(z) > - < C_1(z,t) >)$$

Analogous expression can be written for the internal layers of the sediment. By the same notation, the respective concentration increase in the reducing layer is

$$\Delta < C_2(z,t) >= \frac{\Delta t \pi^2 D_2}{4(z_1 - z_2)^2} (< \underline{C}_2(z) > - < C_2(z,t) >)$$

and that in the anoxic layer results

$$\Delta < C_3(z,t) >= \frac{\Delta t \pi^2 D_3}{4(z_2 - z_3)^2} (< \underline{C}_3(z) > - < C_3(z,t) >)$$

The asymptotes of the three layers are generally obtained by solving the diffusion equation as shown in the appendix.

3. Results

3.1 Single-Layer Sediment

In this section, vertically integrated concentrations of carbon dioxide originate from leakages in different abiotic sediments. The strategy is to analyse separately three main possibilities in real scenarios:

1. The scenario has no carbon dioxide fluxes entering the layer and the ecosystem evolves in the presence of the environmental conditions, which are generally subject to natural and anthropic variability;

2. The CO_2-laden water is released through the bottom of the sediment and, after interacted with the sediment complex, is transported towards the water column which insists on the corresponding area of the seabed: in specific sites studied in the Tyrrhenian Sea, diffuse sources carry 0.1 mmol C m^{-2} s^{-1} with upward velocity of about 6.3 10^{-7} m s^{-1} into the Mediterranean seawater (Hall-Spencer et al., 2008; Caramanna et al., 2011);

3. CO_2 leakage enters the bottom of the sediment with diffusive release into the water column over a large area and this approach allows for the assumption of lateral loads and homogeneous structural parameters: in this work, the selected loss values can double CO_2 concentrations in porous sediment water and these constant upward fluxes

range from 0.002 to 0.012 mmol C m^{-2} s^{-1} in cases of depth of the sediment layer ranging, respectively, from 0.5 m to 0.1 m.

These three scenarios are consistent, respectively, with a normal evolution scenario, one with high flux and both advective and diffusive leaks, and low flux scenarios, i.e. cases of diffusive transudation. The equilibria concentrations are calculated with constant and continuous losses of carbon dioxide: no inputs, leakage, and absorption of CO_2 in the reactive layer. Carbon dioxide concentrations and vertical integrations of the contents are evaluated, originating from leakages in different sediments. The equilibrium concentrations follow three cases: no input; specified carbon dioxide leakage; the same loss specified in the previous case, but with additional homogeneous absorption equal to the entrance input. The porosity φ is 0.5, in the typical range of clay and sand from 0.4 to 0.6, and the diffusion constant, *D*, is 5.4 10^{-10} m^2 s^{-1}.

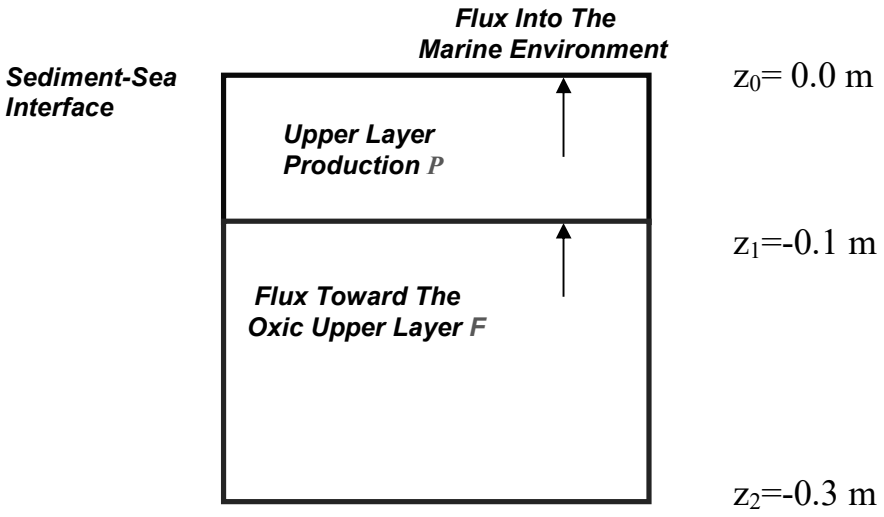

Fig. 2. Single-layer parameters.

In Fig. 2 the sediment-sea interface is at depth z_0=0 m with the production S in the upper layer U, 0.1 m thick, and the flux into the upper layer from the middle layer M, 0.2 m thick as well as the deeper layer D. The flux to the marine environment and the concentration of the upper layer are calculated from the previous data using the diffusion coefficient and concentration of the sediment-sea interface. In the case of the 0.1 m layer with interface concentration C_0=2300 mmol C m^{-3} and null fluxes, there is no input from the bottom of the sediment, F=0, and the net production of carbon, S, sum of all sources and sinks in the layer, is zero.

The reference concentration at the bottom of the layer, C_1, and the vertically integrated concentration, $\underline{C}_1$, result:

$$\begin{cases} C_1 = \underline{C}(z = L) = 2300 mmolCm^{-3} \\ \underline{C}_1 = L < \underline{C}(z) >= \phi \cdot 2300 mmolCm^{-3} \cdot 0.1m = 115.0 mmolCm^{-2} \end{cases}$$

In the second case, the carbon dioxide leakage F from the middle layer is 0.01 μmol C m^{-3} s^{-1}, and the steady-state boundary concentration and content are:

$$\begin{cases} C_1 = \dfrac{0.00001 mmolCm^{-2}s^{-1}(z_0 - z_1)}{0.5D} + 2300 mmolCm^{-3} = 6003.7 mmolCm^{-3} \\ \underline{C}_1 = \phi(2300 mmolCm^{-3} + \dfrac{0.00001 mmolCm^{-2}s^{-1}}{0.5D}\dfrac{z_0 - z_1}{2})(z_0 - z_1) = 207.6 mmolCm^{-2} \end{cases}$$

The integrated concentration is almost twice as high, while the concentration at the bottom of the layer is more than twice as high as in the unperturbed layer.

The third case is with the same boundary condition and flux, as in the second case, but with a homogeneous absorption of carbon dioxide in the layer equal to the leakage

$$\begin{cases} C_0 = 2300 mmolCm^{-3} \\ F = 0.01 \mu molm^{-2}s^{-1} \\ S = -0.01 \mu molm^{-2}s^{-1} \end{cases}$$

and in this case the results are

$$\begin{cases} C_1 = \dfrac{F}{0{,}5D}(z_0 - z_1) + \dfrac{S}{D}\dfrac{z_0 - z_1}{2} + C_0 = 5077{,}8 mmolCm^{-3} \\ \underline{C}_1 = \phi\left(C_0 + \dfrac{F}{0{,}5D}\dfrac{z_0 - z_1}{2} + \dfrac{S}{D}\dfrac{z_0 - z_1}{3}\right)\cdot 0{,}1m = 176{,}7 mmolCm^{-2} \end{cases}$$

In this third case, the absorption of carbon dioxide within the 0.1 m upper layer results in a zero flux released to the marine environment and an increase in the average concentration of about 55% compared to the reference scenario; the absorption is able to partially restore the reference concentration of 115 mmol C m^{-2}, with the intermediate value of 176.7 mmol C m^{-2}.

There are two things to note: first, the concentration at the sediment bottom remains very high, over 5000 mmol C m^{-3}, far from the seawater concentration of 2300 mmol C m^{-3}: second, the intermediate equilibrium value achieved by the integrated concentration is closer to the second case with leakage than to the first case with no leakage.

The case of the first 2.1 example is shown in Fig. 3 with D=5.4 10^{-10} m^2 s^{-1} and z_1=0.1 m. In the interval of sixty days shown in Fig. 3, the average concentration reaches an intermediate value between the high initial concentration and the asymptotic concentration. Medium-term simulations, from a few days to several weeks, describe well this environmental situation.

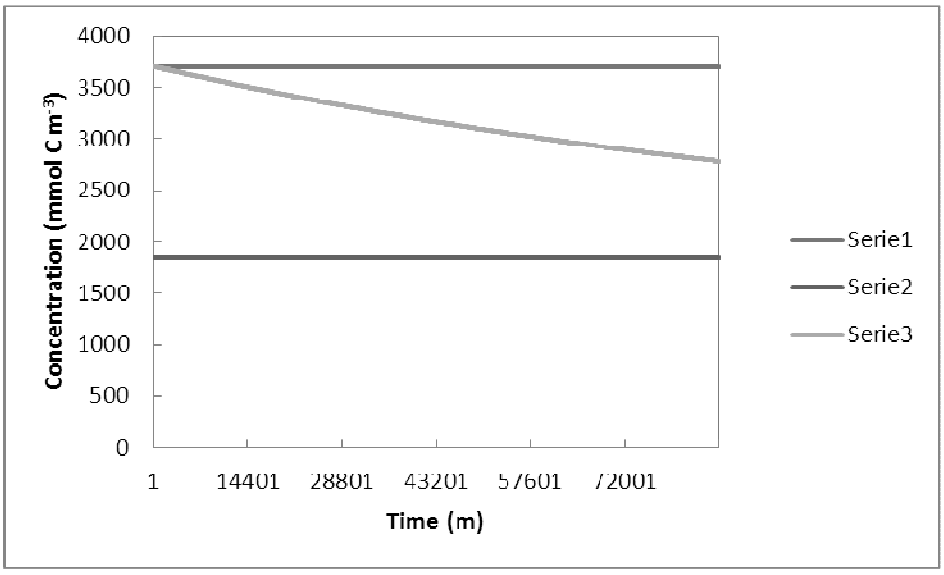

Fig. 3. Average concentrations of the first 2.1 example with ϕ 0.5 and F 0.01 μmol C m^{-2} s^{-1}, starting from the initial condition FL/ϕD, Series 1, to the final asymptotic condition FL/2ϕD, Series 2, through the time evolution of the average concentration in the upper layer over sixty days, Series 3.

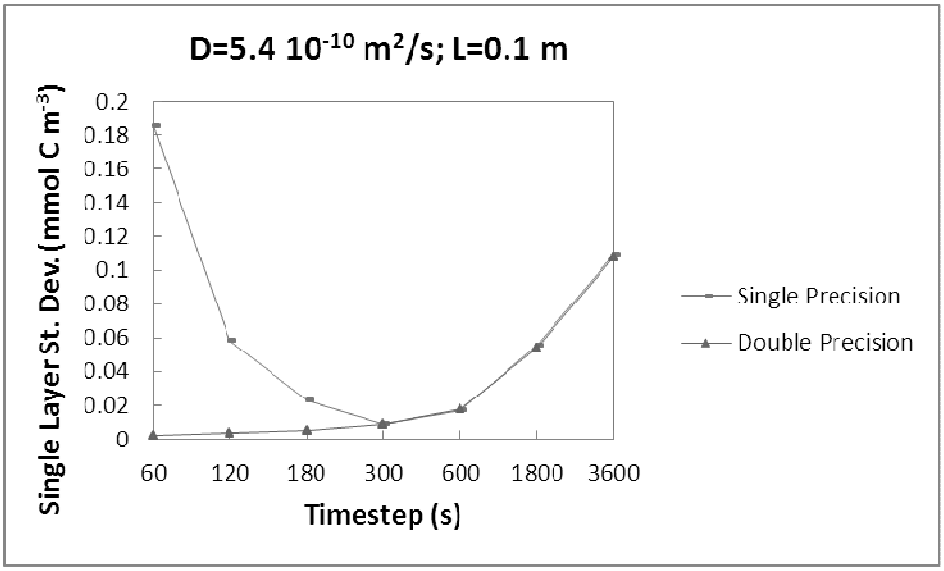

Fig. 4. Standard deviations of the first 2.1 example with respect to the exact solution with single precision, rectangles, and double precision, triangles, in the first year of the simulation.

The time evolution must be followed by the exact solution expanded in Fourier series, see the appendix. The error of the calculation depends on the accuracy with which the calculation is performed (Fig. 4).

For example, in the 0.1 m layer with the same diffusion constant, $D=5.4\ 10^{-10}$ m^2 s^{-1}, the single layer method in the first year gives the standard errors with respect to the exact solution. Therefore, double precision has been chosen for these applications, because higher, extended precision does not improve the standard errors. In the double precision case, we see a reduction in error by reducing the integration step down to 10^{-2} mmol C m^{-3} when the background water concentration in the environment is 2300 mmol C m^{-3}, which corresponds to an accuracy of the method of five orders of magnitude compared

to the average concentrations of the system, with the time step of the simulation set to less than three minutes.

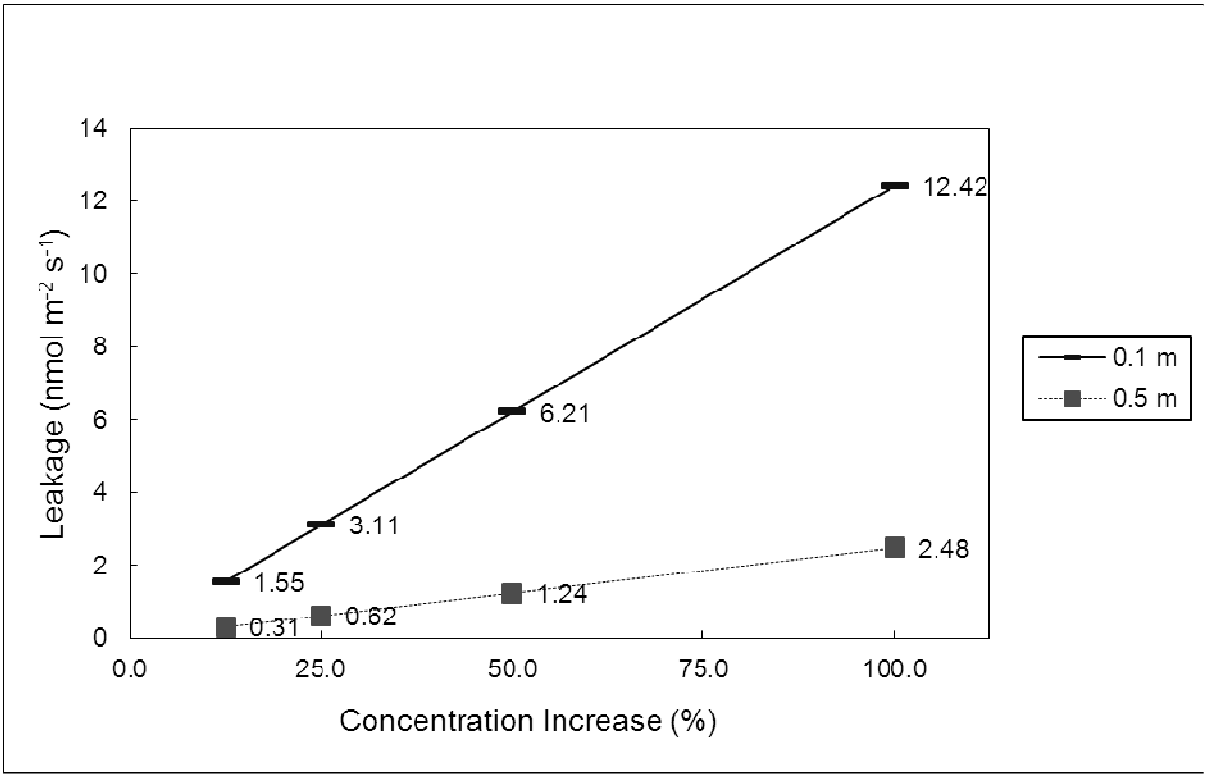

Fig.5. Steady increase of concentration in porewater with D=5.4 10^{-10} m^2 s^{-1}, porosity of 0.5 and seawater concentration of 2300 mmol C m^{-3}; CO_2 leakages are located at the bottom of the sediment, respectively, 10 cm depth, squares, and 50 cm depth, slashes, and their values are reported.

The leakages in Fig. 5 are proportional to the concentration increases in each layer and, due to the same concentration increase in both layers, inversely proportional to the depth ratio of the two layers.

The carbon dioxide fluxes, expressed as positive fluxes from the bottom of the sediment layer to the porewater of the same layer, are applied to the bottom of a layer of 0.1 m: the minimum value is 1.55 nmol C m^{-2} s^{-1} to the maximum value, which is assumed to be 12.42 nmol C m^{-2} s^{-1}. In Fig. 5, the cases of concentrations in layers of 0.1 m and 0.5 m are considered.

3.2 Three-Layer Description

To discuss the possible three-layer abiotic responses, applications with constant inputs as well as inputs of short duration are presented.

Constant applications are made with two leakages: the first, 0.2 mmol C m^{-2} d^{-1}, is applied as a leakage to the sediment bottom and the second, -0.1 mmol C m^{-2} d^{-1}, is absorbed carbon in the upper layer U.

Moreover, the fluxes into the seawater are still negative in the first year of the simulation and increase, and the flux, in the case of uniform diffusion of 0.00015 m^2d^{-1} (Fig. 6b), is significantly greater than that determined with the diffusion constant 0.00005 m^2 d^{-1} (Fig. 6a). With a constant and identical leakage in both diffusion cases, the fluxes of the upper layer in Fig. 6 increase in absolute value but do not reach the value of the internal absorption.

The fluxes toward the seawater become positive after the first year of simulation in the case of high diffusion, while they need more than four years in the second case, where diffusion is reduced to one third. The fluxes in the deepest and middle layers show similar behaviour in both applications. The deeper layer absorbs more than three times as much as the middle layer in the case with the highest diffusion.

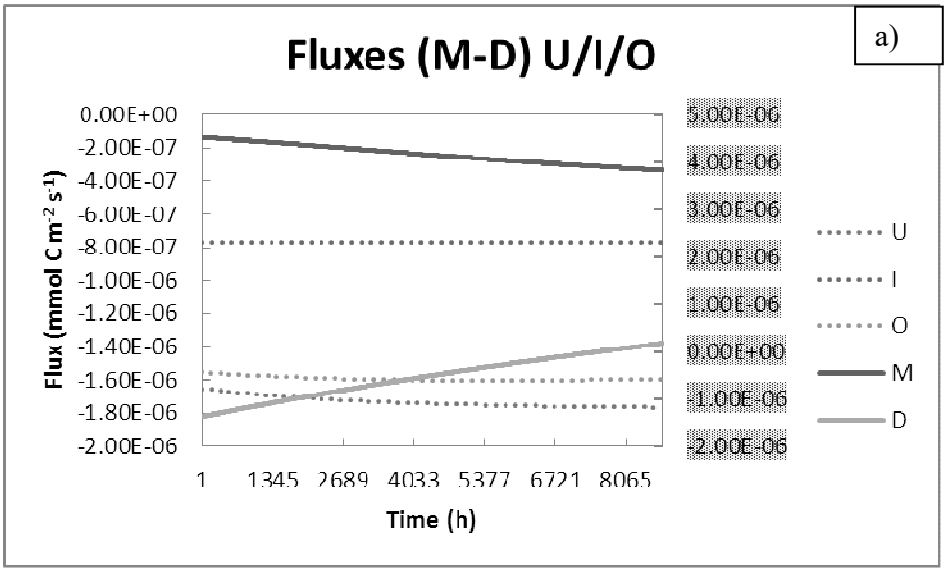

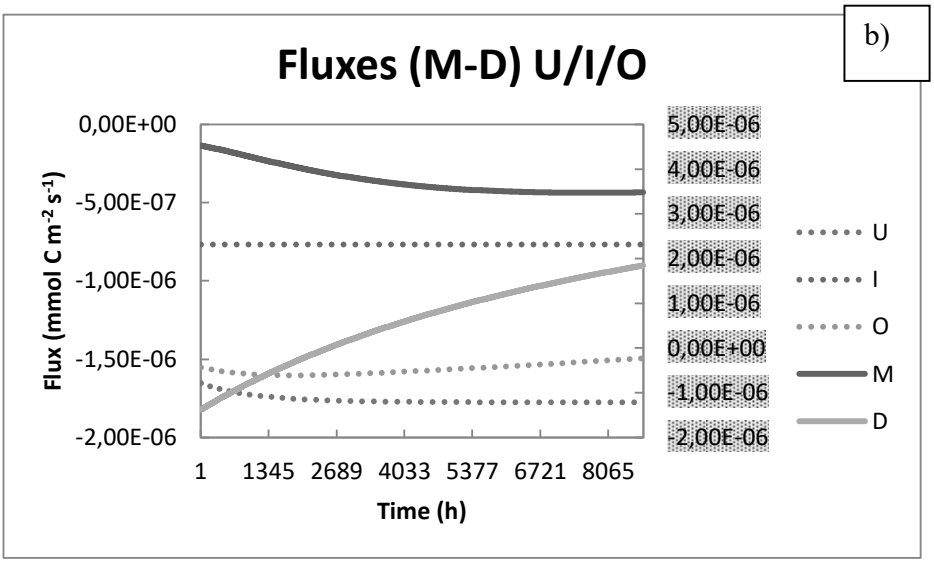

Fig. 6. Fluxes during the first-year simulation with constant flux from the sediment bottom and absorption in the upper layer a) D=0.00005 m^2 d^{-1} e b) D=0.00015 m^2 d^{-1}; left scale for the full lines.

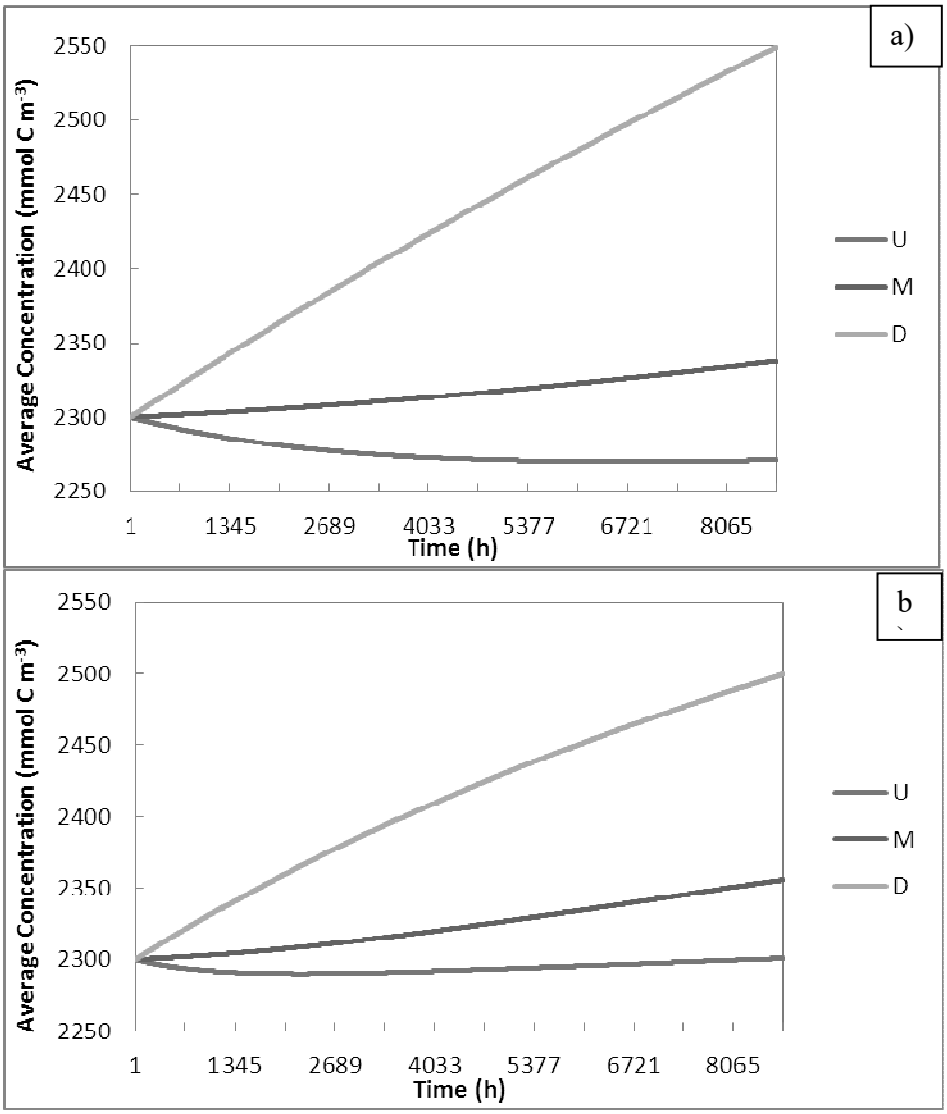

Fig. 7. First-year concentrations in the case of constant flux from the sediment bottom and absorption in the upper layer: a) D=0.00005 m^2 d^{-1} and b) D=0.00015 m^2 d^{-1}.

The one-year simulations of the mean concentrations with the diffusion constants 0.00005 m^2 s^{-1} and 0.00015 m^2 s^{-1} are shown in Fig. 7. The concentrations increase under both environmental conditions and reach higher values for the lower diffusion constant (Fig. 7a) than for the higher one (Fig. 7b).

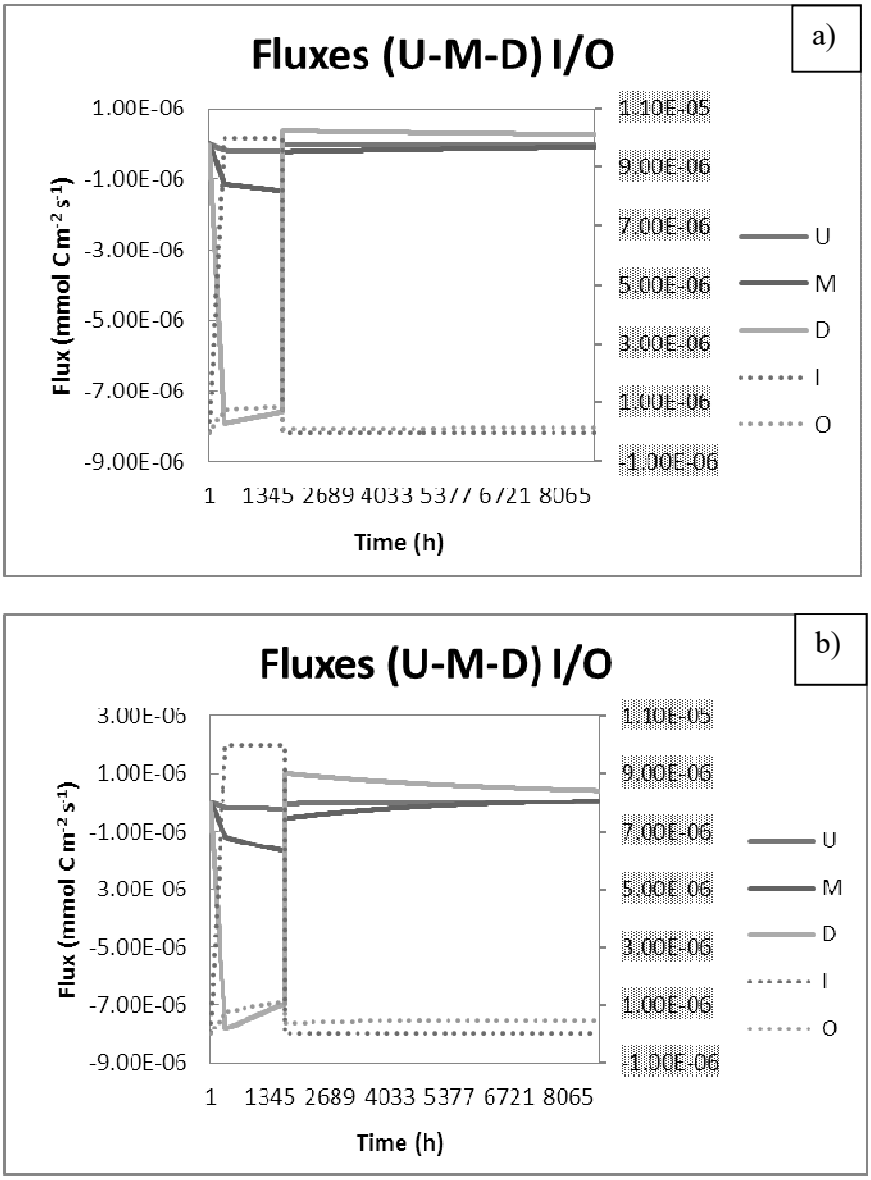

Fig. 8. Fluxes with the eight-week bottom leakage during the first-year simulations with D=0,00005 m^2 d^{-1} and D=0,00015 m^2 d^{-1}; right scale for the dotted lines.

The behaviour of the upper layer U shows a decrease in concentration for the greater influence of the absorption present than for the influence of the outflowing deeper layer D; this behaviour is discussed in the next paragraph by introducing the reference values.

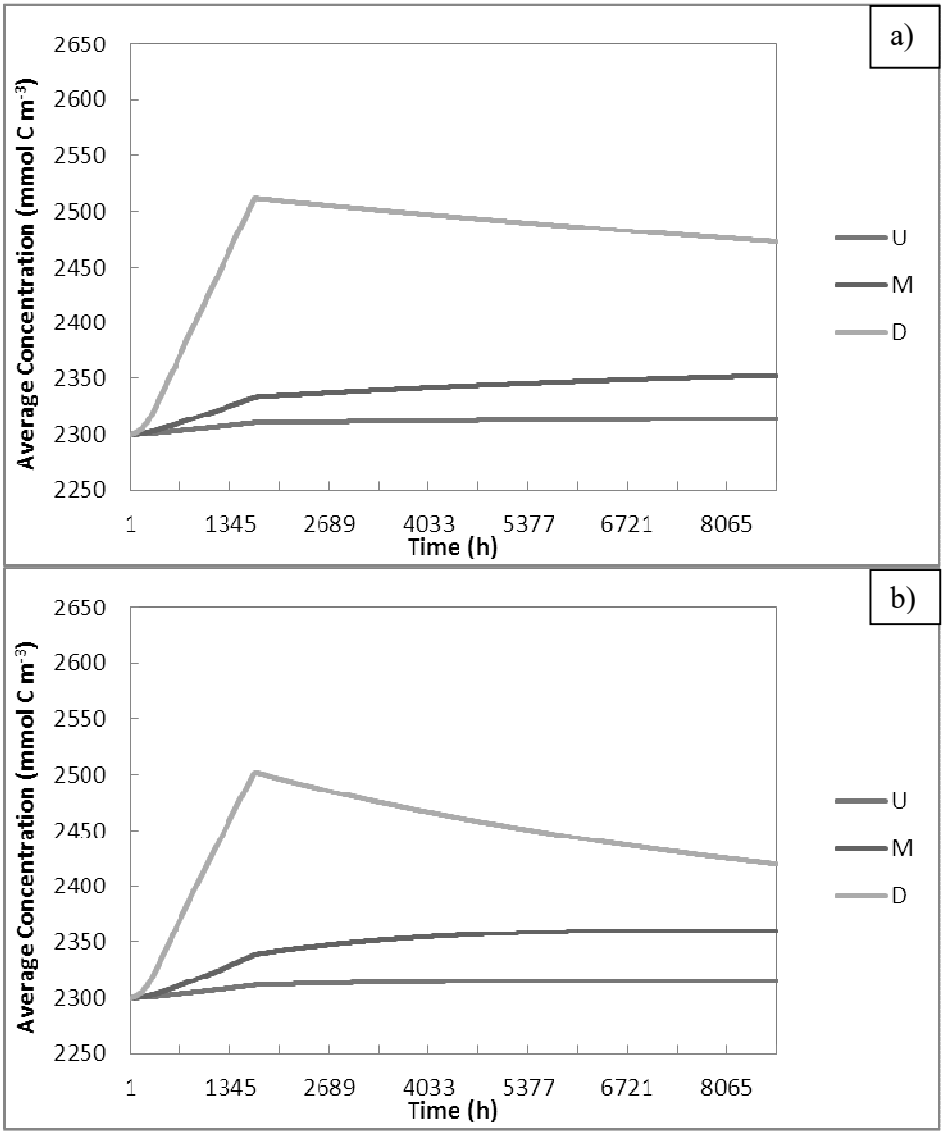

Fig. 9. First-year concentrations during and after the eight-week bottom leakages: a) D=0.00005 m^2 d^{-1} and b) D=0.00015 m^2 d^{-1}.

In deeper layer D and partly also in middle layer M, much higher values are obtained at the end of the first-year simulation. In general, the concentrations are higher in the case with lower diffusion.

The short-term applications include a carbon dioxide leakage of 70 days with linear growth in the first 14 days towards the final constant value of 10 nmol C m^{-2} s^{-1} from the sea bottom; this leakage is maintained for eight weeks, from the fifteenth to the seventieth day, and then reset; in this case, no absorption takes place. The flux values, dashed lines in Fig. 8, show both the input from the sediment and the output towards the seawater, which is maintained at a constant concentration of 2300 mmol C m^{-3}. From the comparison of these dashed lines, it can be seen that the flux of the output in Figure 8b is higher than in the lower dispersion, Figure 8a. Even after the CO_2 input is restored, the former remains about twice as high with respect to the former. Figure 9a shows an increase in concentrations in the three layers, starting from the same value of initially 2300 mmol C m^{-3} and with D=0.00005 m^{-2} d^{-1}. The deeper layer increases more than the upper and middle layers. The increase in concentration is similar to the case of the diffusion constant D=0.00015 m^2 d^{-1} shown in Fig. 9b. The concentrations achieved with the second diffusion constant are lower than those in Fig. 9a. This behaviour is general and also in the context of this study, as far as it is an idealised behaviour, due to the fact that the asymptote depends inversely on the diffusion constant, i.e. the larger the diffusion, the smaller the maximum concentration value. The three-layer concentrations persist even when the CO_2 leakage is eliminated.

3.3 Asymptotic Values and Fluxes

The asymptotes obtained with the absorption of -0.1 mmol C m^{-2} d^{-1} give very different values compared to the values of the transient shown in Figs. 6 and 7.

There is a large difference between the asymptote of 2433.3 mmol C m^{-3} of the upper layer and the transient of this layer U, which remains below the reference value of 2300 mmol C m^{-3} throughout the first-year simulation (Fig. 7a).

In fact, for the case of leakage and absorption in the first layer with D=0.00005 m^{-2} d^{-1}, we obtain

$$\begin{cases} C_0 = 2300 mmolCm^{-3} \\ C_1 = -\dfrac{-0.1}{2 \cdot 0.00005} 0.1 + \dfrac{-0.1 + 0.2}{0.00005} + 2300 mmolCm^{-3} = 2600 mmolCm^{-3} \\ C_3 = \dfrac{0.2}{0.00005} 0.2 + 2600 mmolCm^{-3} = 3400 mmolCm^{-2} \end{cases}$$

Therefore, with

$$\begin{cases} C_0 = 2300 mmolCm^{-3} \\ F = 0.2 mmolCm^{-2} d^{-1} \\ S = -0.1 mmolCm^{-2} d^{-1} \end{cases}$$

we obtain the asymptotic average concentrations

$$\begin{cases} \underline{C}_1 = \dfrac{2\dfrac{-0.1+0.2}{0.00005}+\dfrac{0.2}{0.00005}}{2}\dfrac{0.1}{3}+2300 mmolCm^{-3} = 2433.3 mmolCm^{-3} \\ \underline{C}_2 = \dfrac{2\dfrac{0.2}{0.00005}+\dfrac{0.2}{0.00005}}{2}\dfrac{0.2}{3}+2600 mmolCm^{-3} = 3000 mmolCm^{-3} \\ \underline{C}_3 = \dfrac{2\dfrac{0.2}{0.00005}+\dfrac{0.2}{0.00005}}{2}\dfrac{0.2}{3}+3400 mmolCm^{-3} = 3800 mmolCm^{-2} \end{cases}$$

The asymptotes are shown both in Tab. 1 column 3 in the case of absorption and column 2 in the absence of absorption.

Table 1. Asymptotic average concentrations in mmol C m^{-3} both in seawater and in the layers U, M, and D for the diffusion constant 0.00005 m^{-2} d^{-1}; in parentheses there are the asymptotic average concentrations for the diffusion constant 0.00015 m^2 d^{-1}.

Layer	**0.2 mmol C m^{-2} d^{-1} Constant Leakage Without U Uptake (not shown)**	**0.2 mmol C m^{-2} d^{-1} Constant Leakage With U Uptake -0.1 mmol C m^{-2} d^{-1}**
Seawater Concentration	2300	2300
Layer U	2500 (2367)	2433.3 (2344)
Layer M	3100 (2567)	3000 (2533)
Layer D	3900 (2833)	3800 (2800)

The value of the surface layer U drops below the initial value and well below the asymptote. This behaviour is due to the absorption present only in the layer U, which

accounts for half of the carbon dioxide input, as the flux to the other layers is still low and mainly increases the concentration of the deeper layer D. Part of the carbon dioxide demand comes from the absorption of the layer U from the seawater and part from the decrease in concentration in the upper layer U itself.

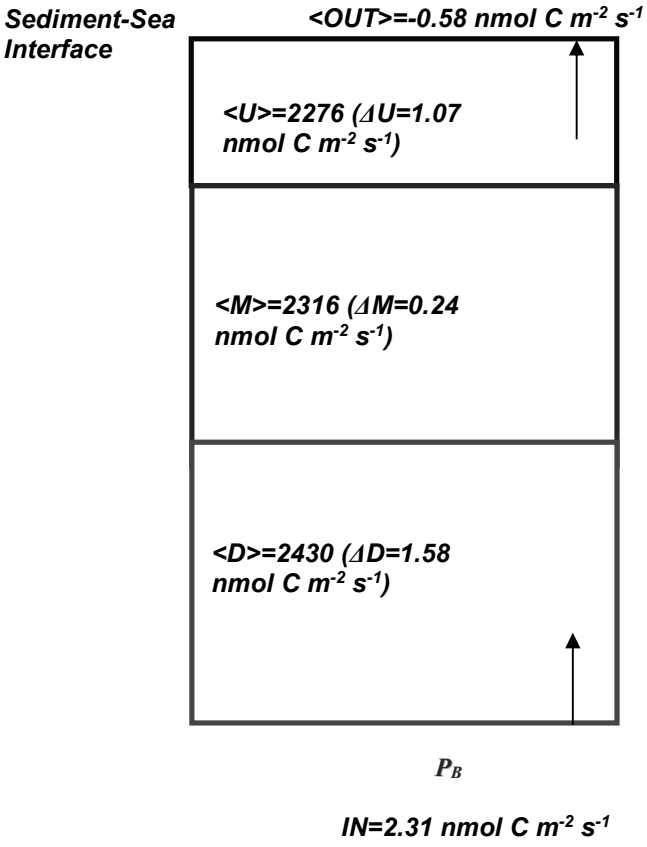

Fig 10. Fluxes during the first-year simulation with constant input, the diffusion constant is 0.00005 m^{-2} d^{-1}.

3.4 Coupled CO_2 and CH_4 Cycles

The main activity of the synthesis developed here is the study of nutrient cycling, mainly carbon cycling, in anoxic and reducing sediment layers. At the same time, the effects of CO_2 on methanogenesis and methanotrophy are investigated as microbially mediated processes, considering the role of sulphur, and the variability of nutrient concentrations in the boundary deeper layer is also characterised.

The inclusion of benthic processes in a clear and unified framework is considered methodologically important. On the other hand, the variability of concentrations in the boundary deeper layer includes specific influences such as currents and stratification.

Carbon dioxide production can mainly occur through the following reactions in seawater and porewater: methanogenesis, dissimilatory reduction of sulphate, dissimilatory reduction of iron, dissimilatory reduction of manganese, denitrification, dissimilatory reduction of nitrate and ammonium (Brandes et al, 2007), aerobic respiration, aerobic oxidation of methane, dissolution of calcite, aragonite, Mg-calcite and other carbonates.

On the other hand, the concepts of inorganic carbon uptake are: primary production, anaerobic oxidation of methane, bacterial production, biological calcification, anaerobic oxidation of ammonia, nitrification, precipitation of calcite, aragonite, Mg-calcite and other carbonates.

The specific role of each reaction must be evaluated to understand the carbon cycle in the ecosystem. After describing these processes, each with its chemical reaction, the

development of abiotic and bacterial sediments is reported; the former serves as a model for biogeochemical cases.

The carbon cycle with carbon dioxide and methane is studied in the geometry of Fig. 1. The following processes have been considered: aerobic respiration, aerobic oxidation of methane AEOM, methanogenesis, sulphate reduction and anaerobic oxidation of methane AOM. Denitrification, manganese reduction and iron reduction are not considered in this application.

In the upper oxygenated layer of the sediment, mineralisation reactions where C/P and N/P are the carbon-phosphorus molar ratio and the nitrogen-phosphorus molar ratio, respectively, are aerobic respiration

$$CH_2O + O_2 \rightarrow CO_2 + H_2O$$

with the half-saturation constant

$$R_O = r \frac{O_2}{k_O + O_2} D_C$$

and AEOM

$$CH_4 + 2O_2 \rightarrow CO_2 + 2H_2O$$

treated as first-order reaction

$$R_{CH4o2} = O_2 k_{mox} CH_4$$

The methanogenesis is regulated by the porewater concentration and, linearly, by the particulated organic matter as follows

$$C_2H_3O_2^- + H^+ \rightarrow CH_4 + CO_2$$

with rate $R_M = r \frac{k_S^{'}}{k_S^{'} + SO_4} \frac{k_N^{'}}{k_N^{'} + NO_3} \frac{k_O^{'}}{k_O^{'} + O_2} D_C$

and is active in the anoxic layer.

Finally, the following expression gives the sulphate reduction with rate dependent on the chemical composition in the sediment

$$2CH_2O + H_2SO_4 \rightarrow 2H_2CO_3 + H_2S$$

and the rate for this equation is

$$R_S = -r \frac{SO_4}{SO_4 + k_S} \frac{k_N^{'}}{k_N^{'} + NO_3} \frac{k_O^{'}}{k_O^{'} + O_2} D_C$$

as the former reaction AOM

$$CH_4 + SO_4^{2-} \rightarrow H_2O + HS^- + HCO_3^-$$

with rate

$$R_{CH4O4} = SO_4 k_{mox} CH_4$$

is present in the middle layer.

Table 2. Geochemical Parameters

Parameter	Definition	Value	Units
R	DOC Remineralization Rate	$5.9\ 10^{-8}$	s^{-1}
k_O	Half-saturation Concentration for Aerobic Respiration	10.	mmol O_2 m^{-3}
k_N	Half-saturation Concentration for Denitrification	30.	mmol N m^{-3}
k_M	Half-saturation Concentration for Manganese Reduction	5000.	mmol Mn m^{-3}
k_F	Half-saturation Concentration for Iron Reduction	$1.25\ 10^4$	mmol Fe m^{-3}
k_S	Half-saturation Concentration for Sulphate Reduction	1620.	mmol S m^{-3}
k_O'	Inhibition Concentration for Denitrification	10.	mmol O_2 m^{-3}
k_N'	Inhibition Concentration for Manganese Reduction	30.	mmolN m^{-3}
k_M'	Inhibition Concentration for Iron Reduction	5000.	mmol Mn m^{-3}
k_F'	Inhibition Concentration for Sulphate Reduction	$1.25\ 10^4$	mmol Fe m^{-3}
k_S'	Inhibition Concentration for Methanogenesis	1620.	mmol S m^{-3}
k_{met}	Methanotrophy Rate	$9.5\ 10^{-7}$	mmol S^{-1} m^3 s-1
k_{mox}	Methane Oxidation Rate	$3.2\ 10^{-5}$	mmol O_2^{-1} m^3 s-1
k_{sox}	Hydrogen Sulphide Oxidation Rate	9.5 10-3	mmol O_2^{-1} m^3 s-1
A_N	Ammonium Adsorption	3.5	
A_P	Phosphate Adsorption	31.5	
ϕ	Porosity	0.55	
D_1	U Diffusion Constant	$5.4\ 10^{-10}$	m^2 s^{-1}
D_2	M Diffusion Constant	$5.4\ 10^{-10}$	m^2 s^{-1}
D_3	D Diffusion Constant	$5.4\ 10^{-10}$	m^2 s^{-1}

Table 3. Initial conditions in seawater, W, and in the layers U, M, and D in mmol m^{-3}.

	DIC	Methane	DOC	Oxygen
W	2300	0.025	400	0.05
U	2300	0.0	400	0.05
M	2300	0.0	600	0
D	2300	0.0	800	0

The initial concentrations of dissolved IC and methane are 2300 mmol C m^{-3} and 0.025 mmol C m^{-3}, respectively: these are the neutral values for carbon dioxide and methane without fluxes.

The simulation time step is 3600 s. In the present application, the CO_2 leakage is 3.0 nmol C m^{-2} s^{-1} from the bottom of the sediment at 0.5 m depth. This leakage is higher than that used in the previous case and corresponds to 1.135 kg m-2 per year.

The initial state of sulphate is fixed at 250 mmol S m^{-3}, nitrate is zero, oxygen is 5 mmol O m^{-3} in the oxygen-rich layer, zero in the middle and deeper layers. Particulate organic carbon is fixed at 400, 600 and 800 mmol C m^{-3} respectively in the three layers from the surface downwards (Herndl et al., 1989).

$$\begin{cases} C_0 = 2300 mmolCm^{-3} \\ C_1 = -\dfrac{3\cdot 10^{-6}}{\phi 5.4\cdot 10^{-10}} 0{,}1 + 2300 mmolCm^{-3} = 3310{,}1 mmolCm^{-3} \\ C_3 = \dfrac{3\cdot 10^{-6}}{\phi 5.4\cdot 10^{-10}} 0{,}2 + 3310{,}1 mmolCm^{-3} = 5330{,}3 mmolCm^{-2} \end{cases}$$

The reference values are, from top to bottom: 2805.1 mmol C m^{-3} for the layer U; 4320.2 mmol C m^{-3} for the layer M; 6340.4 mmol C m^{-3} for the layer D. These reference values are the final values obtained when a constant CO_2 leakage is applied, but with a zero sum S, so that the dynamic sum of all sources and absorptions of carbon dioxide is zero.

$$\begin{cases} C_0 = 2300 mmol Cm^{-3} \\ F = 0.003 \mu mol Cm^{-2} s^{-1} \\ S = Sum(of) Sources(and) Sinks = 0.0 \mu mol Cm^{-3} s^{-1} \end{cases}$$

In fact, we obtain

$$\begin{cases} \underline{C}_1 = \dfrac{2\dfrac{3\cdot 10^{-6}}{5{,}4\cdot 10^{-10}} + \dfrac{3\cdot 10^{-6}}{5{,}4\cdot 10^{-10}}}{2\phi}\dfrac{0{,}1}{3} + 2300 mmol Cm^{-3} = 2805{,}1 mmol Cm^{-3} \\ \underline{C}_2 = \dfrac{2\dfrac{3\cdot 10^{-6}}{5{,}4\cdot 10^{-10}} + \dfrac{3\cdot 10^{-6}}{5{,}4\cdot 10^{-10}}}{2\phi}\dfrac{0{,}2}{3} + 3310{,}1 mmol Cm^{-3} = 4320{,}2 mmol Cm^{-3} \\ \underline{C}_3 = \dfrac{2\dfrac{3\cdot 10^{-6}}{5{,}4\cdot 10^{-10}} + \dfrac{3\cdot 10^{-6}}{5{,}4\cdot 10^{-10}}}{2\phi}\dfrac{0{,}2}{3} + 5330{,}3 mmol Cm^{-3} = 6340{,}4 mmol Cm^{-2} \end{cases}$$

The chemical evolution times of carbon dioxide in the three layers are shown in Fig. 10. The annual release of carbon amounting to 1.135 g C m^{-2} from the sediment bottom at a depth of 0.5 m causes the concentrations in the three sediment layers to increase towards the reference values, so that the final steady-state values are reached after continuous

application of the same CO_2 leakage. These carbon dioxide reference values, reached after about ten years of simulation, are 2805 mmol C m^{-3}, 4320 mmol C m^{-3} and 6340 mmol C m^{-3} for the layers U, M and D, respectively. These final values are steady-state values calculated similarly to the appendix with reduced carbon dioxide fluxes and no other internal sources or sinks, i.e. with source term S zero.

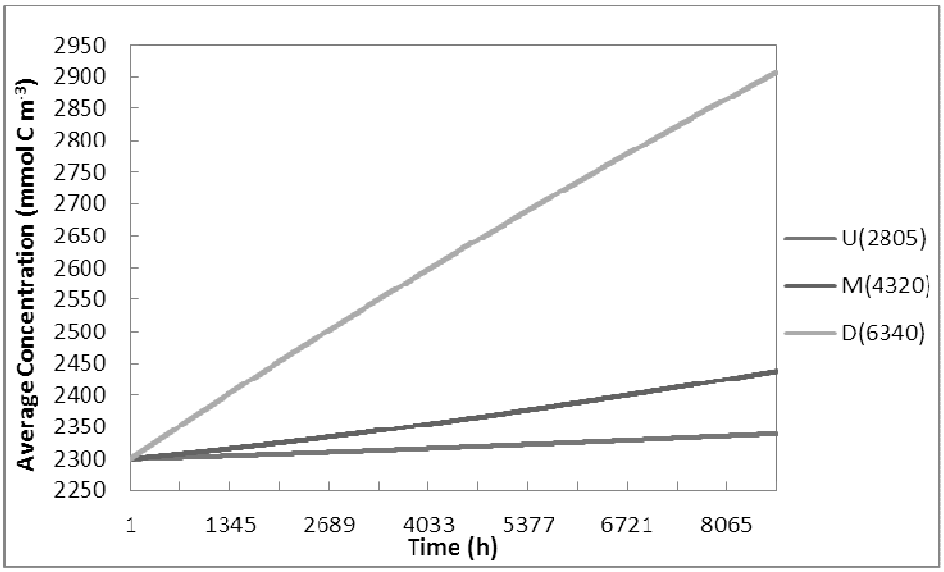

Fig. 11. First-year chemical evolutions of the porewater CO_2 concentrations in the layers U, M, D; diffusion is 5.4 10^{-10} m^{-2} s^{-1}, Φ=0.55, the leakages of CH_4 and CO_2 are 0.0 e 3.0 nmol C m^{-2} s^{-1}, respectively; the reference values are in the legend.

In the purely chemical case, the carbon dioxide concentration of the layer D tends to rise above the undisturbed neutral value (Fig. 11, legend). This is due to the importance of the flux from the base of the sediment, which leads to a greater increase in concentration at depth. The other two layers reach much lower concentrations in the upper layer U and

intermediate concentrations in the layer M. After a few years, the layer U also reaches a concentration of more than 500 mmol C m^{-3} above the undisturbed neutral CO_2 value, which is determined by the sole contact with the water mass of the seabed.

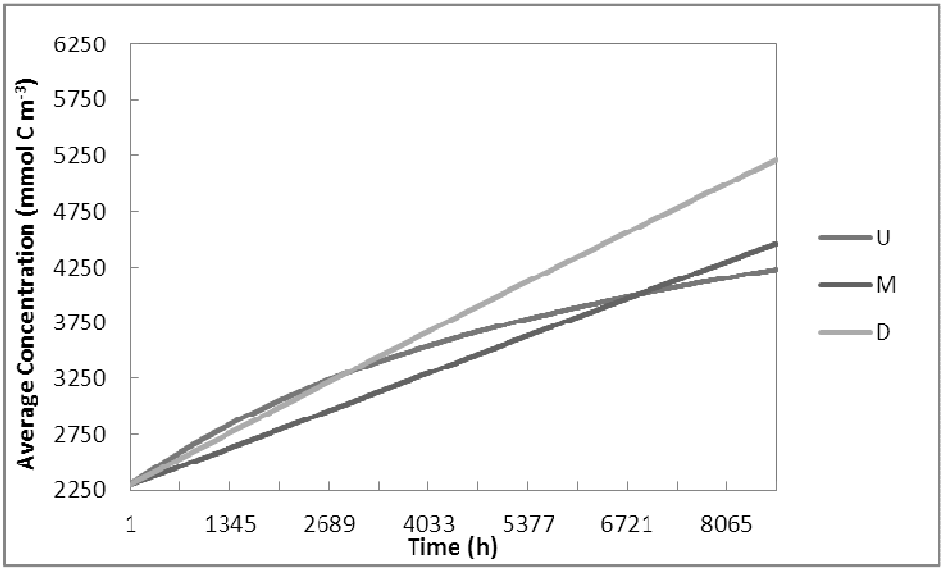

Fig. 12. First-year biotic evolutions of the porewater CO_2 concentrations in the three sediment layers U, M, D; the diffusion constant is 5.4 10^{-10} m^{-2} s^{-1}, Φ=0.55, the bottom leakages are 0.0 and 3.0 nmol C m^{-2} s^{-1} for CH_4 and CO_2, respectively.

When both releases and biogeochemical fluxes are taken into account, CO_2 concentrations show realistic values determined in the marine ecosystem model (Fig. 12).

In the first twelve weeks, the layer U reaches values that are higher than the baseline concentrations. This is due to the strong influence of aerobic respiration whose

contribution is initially greater than that resulting from the leak of CO_2 applied to the bottom of the sediment. In the next phase, during the first year of the simulation, the concentrations in both the middle layer and the deeper layer exceed the concentration value of the layer U; both concentrations in the layers M and D reach values in five years that are about twice as high as the respective reference values already treated in the chemical case, namely 11062 and 14357 mmol C m^{-3}, respectively.

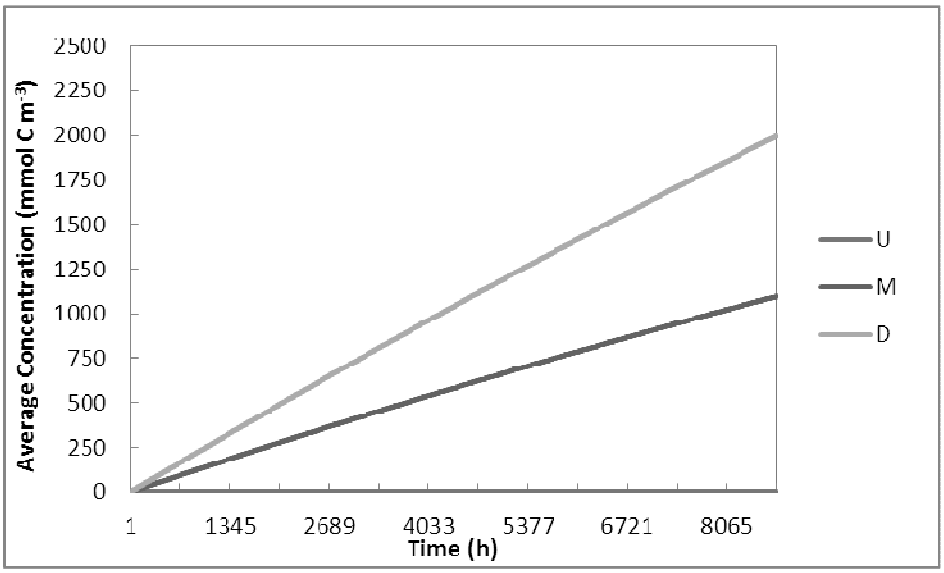

Fig. 13. First-year biotic evolutions of porewater CH_4 concentrations in the three sediment layers U, M, and D; the diffusion constant is 5.4 10^{-10} m^{-2} s^{-1}, Φ=0.55, and the leakages are 0.0 e 3.0 nmol C m^{-2} s^{-1} for CH_4 and CO_2, respectively.

A visual inspection of the behaviour of methane in Fig. 13 during the first year of the simulation shows that concentrations reach high values comparable to those of carbon

dioxide, except in the upper layer U. In fact, the upper layer U remains at a value of 1.45 mmol C m^{-3} CH_4 in the pore water, which is slightly above the neutral value of 0.025 mmol C m^{-3} for methane. On the other hand, significant amounts of methanogenesis are concentrated in the middle layer M and the deeper layer D, reaching over 1000 and 2000 mmol C m^{-3}, respectively, after one year of evolution.

Appendix

The diffusion equation with zero-order reactor is as follows

$$\frac{\partial^2 C}{\partial z^2} = \frac{1}{D}\frac{\partial C}{\partial t} + f(z,t) \qquad \textbf{(A.1)}$$

With initial profile C(z,0)=φ(z) for 0 ≤ z ≤ L, initial condition, and values C(0,t)=A(t) and C(L,t)=B(t) for t≥0, Dirichlet boundary conditions (Amerio, 1976).

The Fourier expansion in $\sin(\beta_n z)$ has norm 2/L and $\sin(\beta_n L)$ is zero in the zeros $\beta_n L = n\pi$, so $\beta_n = n\pi/L$.

From the Fourier series we get the solution

$$C(z,t) = \sum_{n=1}^{\infty} C_n(t) \sin\frac{n\pi}{L} z \qquad \textbf{(A.2)}$$

With Fourier coefficients given by

$$C_n(t) = \frac{2}{L}\int_0^L dz C(z,t) \sin\frac{n\pi}{L} z \qquad \textbf{(A.3)}$$

To obtain the coefficient $C_n(t)$, we multiply both sides of the partial differential equation time $(2/L)\sin(n\pi z/L)$ and integrate in the interval 0 ≤ z ≤ L.

We obtain, the second-order partial differential equation after integrating twice:

$$\frac{2}{L}\int_0^L dz \frac{\partial^2 C(z,t)}{\partial z^2} \sin\frac{n\pi}{L} z = \frac{2n\pi}{L^2}[A(t) - (-1)^n B(t)] - \frac{n^2\pi^2}{L^2} C_n(t)$$

Applying the rule of the derivative under the integral sign, the other terms become

$$\frac{2}{DL}\int_0^L dz\left[\frac{\partial C(z,t)}{\partial t} - Df(z,t)\right]\sin\frac{n\pi}{L}z = \frac{1}{D}\frac{dC_n(t)}{dt} + f_n(t)$$

after the definition

$$f_n(t) = \frac{2}{L}\int_0^L dz f(z,t)\sin\frac{n\pi}{L}z$$

Thus $C_n(t)$ satisfies the first-order linear differential equation

$$\frac{dC_n(t)}{dt} = -\frac{n^2\pi^2 D}{L^2}C_n(t) + \frac{2n\pi D}{L^2}[A(t) - (-1)^n B(t)] - Df_n(t)$$

and the integration with respect to time

$$C_n(t) = e^{-t\frac{n^2\pi^2 D}{L^2}}\left\{H_n + D\int_0^t d\tau\left[\frac{2n\pi}{L^2}A(\tau) - (-1)^n\frac{2n\pi}{L^2}B(\tau) - f_n(\tau)\right]e^{\tau\frac{n^2\pi^2 D}{L^2}}\right\}$$

For the initial concentration

$$C_n(t=0) = H_n$$

and for the initial condition

$$C_n(t=0) = \frac{2}{L}\int_0^L dz\varphi(z)\sin\frac{n\pi}{L}z = \frac{2}{L}\varphi_L$$

we obtain the expression

$$C_n(t) = \frac{2}{L}e^{-t\frac{n^2\pi^2 D}{L^2}}\int_0^L dz\varphi(z)\sin\frac{n\pi}{L}z + D\int_0^t d\tau\left\{\frac{2n\pi}{L^2}[A(\tau) - (-1)^n B(\tau)] - f_n(\tau)\right\}e^{(\tau-t)\frac{n^2\pi^2 D}{L^2}}$$

that gives the solution of equation A.1 under the given conditions.

For each time t, the explicit solution is

$$C(z,t)=\sum_{n=1}^{\infty}C_n(t)\sin\frac{n\pi}{L}z=$$

$$=\frac{2}{L}\sum_{n=1}^{\infty}e^{-t\frac{n^2\pi^2D}{L^2}}\sin\frac{n\pi}{L}z\left\{\int_0^L dz\varphi(z)\sin\frac{n\pi}{L}z+D\int_0^t d\tau\left[\frac{n\pi}{L}A(\tau)-(-1)^n\frac{n\pi}{L}B(\tau)-\int_0^L dzf(z,\tau)\sin\frac{n\pi}{L}z\right]e^{\tau\frac{n^2\pi^2D}{L^2}}\right\}$$

and represents the evolution of the 2.1 second example.

For the long-term evolution, the solution of this expression for the steady-state concentration is obtained asymptotically and is maintained by the ecosystem.

To obtain it, we constrain the summation behaviour

$$\sum_{n=1}^{\infty}e^{-tn^2\pi^2D/L^2}\sin\frac{n\pi}{L}z$$

By substituting as unitary the sinusoidal coefficients

$$\sum_{n=1}^{\infty}e^{-tn^2\pi^2D/L^2}\sin\frac{n\pi}{L}z\le\sum_{n=1}^{\infty}e^{-tn^2\pi^2D/L^2}$$

This inequality is valid for all the sine values.

$$\sum_{n=1}^{\infty}e^{-tn^2\pi^2D/L^2}=$$

$$=e^{-t\pi^2D/L^2}+e^{-t4\pi^2D/L^2}\sum_{n=2}^{\infty}e^{-t(n-2)(n+2)\pi^2D/L^2}=$$

$$=e^{-t\pi^2D/L^2}+e^{-t4\pi^2D/L^2}\left(1+\sum_{n=3}^{\infty}e^{-t(n-2)(n+2)\pi^2D/L^2}\right)$$

Considering that for $\alpha>\beta$ follows

$$e^{-\alpha}<e^{-\beta}$$

and that for n>3 it follows

$$n^2 - 4 \geq (n-1)^2$$

the final inequality is

$$\sum_{n=1}^{\infty} e^{-tn^2\pi^2 D/L^2} \sin\frac{n\pi}{L} z \leq$$

$$\leq e^{-t\pi^2 D/L^2} + e^{-t4\pi^2 D/L^2}\left(1 + \sum_{n=3}^{\infty} e^{-t(n-1)^2\pi^2 D/L^2}\right)$$

The second series in the inequality is convergent because it follows from the D'Alembert criterion that

$$\frac{a_{n+1}}{a_n} = \frac{e^{-tn^2\pi^2 D/L^2}}{e^{-t(n-1)^2\pi^2 D/L^2}} = e^{-t(2n-1)\pi^2 D/L^2} \to 0$$

for n going to infinity. The initial series is therefore convergent to the first-order term of a time-negative exponential function, a first-order infinitesimal term of the time step and a quartic-order infinitesimal term of the same time function.

The renewal of the variable *C(z,t)* after the period *t+Δt* is

$$C(z,t+\Delta t) = \frac{2}{L} e^{-t\pi^2 D/L^2}(1-\Delta t\pi^2 D/L^2)\sin\frac{\pi}{L} z\left\{\varphi_L + \int_0^t d\tau(1+\Delta t\pi^2 D/L^2) e^{\tau\pi^2 D/L^2}\left[\frac{\pi D}{L} A(\tau) + \frac{\pi D}{L} B(\tau) - \frac{L}{2} f_1\right]\right\}$$

with both factors at first-order approximation in the time increment.

The cross-product term with $(\Delta t)^0$ gives C(z,t)

$$\frac{2}{L}e^{-t\pi^2 D/L^2}\sin\frac{\pi}{L}z\left\{\varphi_L+\int_0^t d\tau e^{\tau\pi^2 D/L^2}\left[\frac{\pi D}{L}A(\tau)+\frac{\pi D}{L}B(\tau)-\frac{L}{2}f_1\right]\right\}=C(z,t)$$

Finally, the cross-product terms in $(\Delta t)^2$ are higher order infinitesimals and therefore do not contribute to this first order approximation.

Thus, the first-order time increment at $(\Delta t)^1$ results from

$$-\frac{2}{L}e^{-t\pi^2 D/L^2}\Delta t\pi^2 D/L^2\sin\frac{\pi}{L}z\left\{\varphi_L+\int_0^t d\tau e^{\tau\pi^2 D/L^2}\left[\frac{\pi D}{L}A(\tau)+\frac{\pi D}{L}B(\tau)-\frac{L}{2}f_1\right]\right\}=-\Delta t\pi^2 DC(z,t)/L^2$$

multiplying the initial value by the coefficient $-\pi^2 D/L^2$.

Finally, the second first-order term $(\Delta t)^1$ multiplies the time integrated terms

$$\frac{2}{L}e^{-t\pi^2 D/L^2}\sin\frac{\pi}{L}z\left\{\int_0^t d\tau\Delta t\pi^2 D/L^2 e^{\tau\pi^2 D/L^2}\left[\frac{\pi D}{L}A(\tau)+\frac{\pi D}{L}B(\tau)-\frac{L}{2}f_1\right]\right\}=\Delta t\,\pi^2 DC_S(z,t)/L^2$$

yielding the stationary solution, $C_S(z,t)$, by the coefficient $\Delta t\pi^2 D/L^2$ and is independent of the initial condition, which also does not contribute to this term.

Defining the asymptote $\underline{C}(z)=\lim_{t\to\infty}C_S(z,t)$, we obtain the first-order approximation in $(\Delta t)^1$ as the long-term solution for $t>>L^2/\pi^2 D$ given in the text,

$$C(z,t+\Delta t)=C(z,t)+\Delta t(\pi^2 D/L^2)\underline{C}(z)-\Delta t(\pi^2 D/L^2)C(z,t)$$

We assume that the system starts with a homogeneous initial concentration, $C(z,0)=C_0$, and that $f(z,t)=-S/LD$.

The steady-state solution of the time-independent partial differential equation with the sum of all internal sources and sinks, S in mmol C m^{-3} s^{-1}, i.e. the primary production vertically integrated along the layer, which is considered constant in time in the following, and with the time-independent boundary concentrations A and B is

$$D\frac{\partial^2 C}{\partial z^2}+\frac{S}{L}=0$$

Thus, in this notation

$$f(z,t)=f=-\frac{S}{LD}$$

The general solution is

$$C(z)=-\frac{S}{2DL}z^2+az+b$$

and a and b result

$$a=\frac{B-A}{L}+\frac{S}{2D}$$
$$b=A$$

Inserting these values, the stationary solution is

$$C(z)=-\frac{S}{2DL}z^2+\left(\frac{B-A}{L}+\frac{S}{2D}\right)z+A$$

On the other hand, the long-term Fourier integration requires the term f_n which is

$$f_n = \frac{2}{L}\int_0^L dz\left(-\frac{S}{LD}\right)\sin\frac{n\pi}{L}z =$$

$$= -\frac{2S}{L^2 D}\int_0^L dz \sin\frac{n\pi}{L}z =$$

$$= \frac{2S}{n\pi LD}\left(-\cos\frac{n\pi}{L}z\right)\Big|_0^L = \frac{2S}{n\pi LD}[(-1)^n - 1]$$

The solution considering $t>>L^2/D\pi^2$ is the series summation

$$C(z,t) = \sum_{n=1}^{\infty} e^{-t\frac{n^2\pi^2 D}{L^2}}\frac{2C_0}{n\pi}[1-(-1)^n] + \sum_{n=1}^{\infty}\left(1-e^{-t\frac{n^2\pi^2 D}{L^2}}\right)(1-e^{t-\frac{n^2\pi^2 D}{L^2}})\left(\frac{2}{n\pi}A - \frac{2}{n\pi}(-1)^n B - \frac{2LS}{n^3\pi^3 D}((-1)^n - 1)\right)\sin\frac{n\pi}{L}z$$

where C_0 is the homogeneous initial condition and A, B, S are the boundary condition at the top of the layer, the boundary condition at the bottom of the layer, the vertically integrated sum of all sources and sinks in the layer, respectively. The first series does not contribute to the long-term integration; the other three series provide the following positive contributions to the asymptotic concentration:

a) First term

$$\sum_{n=1}^{\infty}\frac{2A}{n\pi}\sin\frac{n\pi}{L}z =$$

$$= \frac{2A}{\pi}\sum_{n=1}^{\infty}\frac{1}{n}\sin\frac{n\pi}{L}z =$$

$$= \frac{2A}{\pi}\frac{\pi - \frac{\pi z}{L}}{2} = A - \frac{Az}{L}$$

b) Second term

$$-\sum_{n=1}^{\infty}\frac{2B}{n\pi}(-1)^n \sin\frac{n\pi}{L}z =$$
$$=\frac{B}{\pi}\sum_{n=1}^{\infty}\frac{2(-1)^{1+n}}{n}\sin\frac{n\pi}{L}z =$$
$$=\frac{B}{\pi}\frac{\pi z}{L}=\frac{Bz}{L}$$

c) Third term

$$\sum_{n=1}^{\infty}\left(-\frac{L^2}{n^2\pi^2}f_n\right)\sin\frac{n\pi}{L}z =$$
$$=\frac{2LS}{\pi^3 D}\sum_{n=1}^{\infty}\frac{1}{n^3}[1-(-1)^n]\sin\frac{n\pi}{L}z =$$
$$=\frac{4LS}{\pi^3 D}\sum_{n=1}^{\infty}\frac{1}{(2n-1)^3}\sin\frac{(2n-1)\pi}{L}z =$$
$$=\frac{4LS}{\pi^3 D}\frac{\pi}{8}\frac{\pi z}{L}\left(\pi-\frac{\pi z}{L}\right)=\frac{Sz}{2D}\left(1-\frac{z}{L}\right)$$

If we combine all the power terms of the spatial variable z, we obtain q.e.d., the asymptotic solution

$$C(z,t)=C(z)=A-\frac{Az}{L}+\frac{Bz}{L}+\frac{Sz}{2D}\left(1-\frac{z}{L}\right)=$$
$$=-\frac{S}{2DL}z^2+\left(\frac{B-A}{L}+\frac{S}{2D}\right)z+A$$

This is equal to the stationary solution obtained without the time-derivative term in the partial differential equation.

The difference from the text expression arises from the substitution of π/2 instead of π in the above solution because the orthogonal functions are given as half-periods in this appendix and quarter-periods in the text solution for the two consistent boundary conditions: due to the two different and consistent boundary conditions, i.e. a pair of Dirichlet conditions here versus mixed Dirichlet-Neumann conditions in the text.

In the 2.1 first example, the transformation of the diffusion term after integration along z is

$$\frac{2}{L}\int_0^L dz \frac{\partial^2 C(z,t)}{\partial z^2}\sin\frac{(2n-1)\pi}{2L}z =$$
$$= (-1)^{n+1}\frac{2}{L}\frac{F(t)}{\phi D} - \frac{(2n-1)\pi}{L^2}\int_0^L dz \frac{\partial C(z,t)}{\partial z}\cos\frac{(2n-1)\pi}{2L}z$$

If we integrate along z the second time, we get

$$\frac{2}{L}\int_0^L dz \frac{\partial^2 C(z,t)}{\partial z^2}\sin\frac{(2n-1)\pi}{2L}z =$$
$$= (-1)^{n+1}\frac{2}{L}\frac{F(t)}{\phi D} + \frac{(2n-1)\pi}{L^2}A(t) - \frac{(2n-1)^2\pi^2}{4L^2}C_n(t)$$

And if we write the solution in terms of C_n, we get

$$C(z,t) = \sum_{n=1}^{\infty} C_n(t)\sin\frac{(2n-1)\pi}{2L}z =$$
$$= \frac{2}{L}\sum_{n=1}^{\infty} e^{-t\frac{(2n-1)^2\pi^2 D}{4L^2}}\sin\frac{(2n-1)\pi}{2L}z\left\{\int_0^L dz\varphi(z)\sin\frac{(2n-1)\pi}{2L}z + D\int_0^t d\tau\left[\frac{(2n-1)\pi}{2L}A(\tau) + (-1)^{n+1}\frac{F(\tau)}{\phi D} - \int_0^L dz f(z,\tau)\sin\frac{(2n-1)\pi}{2L}z\right]e^{\tau\frac{(2n-1)^2\pi^2 D}{4L^2}}\right\}$$

Using the same notation, but under the conditions of 2.2 and in the 2.1 first example, we get the asymptotic solution

$$C(z) = -\frac{S}{2DL}z^{2} + \frac{S}{D}z + \frac{F}{\phi D}z + A$$

With the seawater concentration A and the inflowing flux F from the bottom of the layer. As in the Dirichlet case solved above, S is the sum of all sources and sinks in the layer, where the thickness L of the layer and its porosity Φ, with the diffusion D in the layer, are taken into account.

Plate 1.

Position of the CO_2-Geo scheme in the geochemical matrix; vertical shifts of the different model zones are shown in the three different environments: Atmosphere, Seawater Column and Benthos (top-down Air-Sea-Sediment); relevant processes and research activities are indicated next to each zone. The topics of CO_2-Geo concern the temporal and spatial variability of gas concentrations in benthic habitats and the description of sediment evolution: in the aerobic zone with the oxidation of methane and the biological uptake of carbon, nitrogen, phosphorus, silica; in the sulphate and nitrate reducing zone with the methanotrophic processes; in the anaerobic zone with methanogenetic processes. The subtasks of the systems model consist of four top-down segments: carbon fluxes between air and sea, ecology of the photic zone, description of the bottom boundary layer, geochemistry of the sediments.

<table>
<tr><th>TOPICS
PHASES</th><th>ZONES</th><th>PROCESSES</th><th colspan="2">ACTIVITIES</th></tr>
<tr><td>Air</td><td>TROPOSPHERE</td><td>AIR-SEA CARBON FLUXES</td><td colspan="2" rowspan="2">Fluxes developed using and extending results of the European Union Mediterranean Targeted Project</td></tr>
<tr><td>ea</td><td>PHOTIC ZONE</td><td>NATURAL COUPLING OF CO_2 AND NUTRIENT CYCLES</td></tr>
<tr><td>S</td><td>BOTTOM BOUNDARY LAYER</td><td>TIME AND SPACE VARIABILITIES OF GAS CONCENTRATION IN BENTHOS HABITAT</td><td>BBL</td><td rowspan="4">Integrated here through CO_2-Geo</td></tr>
<tr><td>nt</td><td>AEROBIC ZONE</td><td>BIOLOGICAL UPTAKE OF C, N, P, Si</td><td>OXIC</td></tr>
<tr><td>dime</td><td>SULPHATE REDUCING ZONE</td><td>METHANOTROPHY:
$SO_4^{2-} + CH_4 \rightarrow H_2O + HS^- + HCO_3^-$</td><td>REDOX</td></tr>
<tr><td>Se</td><td>ANAEROBIC ZONE</td><td>METHANOGENESIS:
$CO_2 + 4H_2 \rightarrow CH_4 + 2\,H_2O$</td><td>ANOXIC</td></tr>
</table>

Acknowledgements

The benthic module has been developed and used as a foreground of the European Union 502816 - Network of Excellence on Geological Sequestration of CO_2 during specific studies in the accepted Joint Research Application Proposal 4: Ecosystem Responses to CO_2 Leakage – Model Approach.
This European Union CO_2GeoNet foreground, called CO_2-Geo – "CO_2 Geo" in the proposal – as a background carbon model in the oceanographic 2-phase geochemistry of a later European Union project, is here defined and verified in first-order contexts by the technical details given in the appendix.
The contents not fully developed before in the Figs. 3–13 are attributable only to this work, as a spin-off of the European Union 240837-Research into Impacts and Safety in CO_2 Storage using English as the working language and counting: 13 R&D, 5 Industrial, and 4 Consulting Partners.
This work is the unabridged and revised derivation from the Crispi (2022) foreground of the former project.

References

Amerio, L., 1976. Analisi matematica con elementi di analisi funzionale: Volume II. Tamburini Masson Editori, Centro Grafico Linate, Milano, IT, 503–538.

Blackford, J. C., 2002. The Influence of Microphytobenthos on the Northern Adriatic Ecosystem: A Modelling Study. Est. Coast. Shelf Sci., 55(1), 109–123.

Boetius, A., Ravenschlag, K., Schubert, C. J., Rickert, D., Widdel, F., Gieseke, A., Amann, R., Jørgensen, B. B., Witte, U., Pfannkuche, O., 2000. A marine microbial consortium apparently mediating anaerobic oxidation of methane. Nature, 407, 623–626.

Boudreau, P. B., 1996. A method-of-lines code for carbon and nutrient diagenesis in aquatic sediments. Comp. Geosci., 22(5), 479–496.

Brandes, J. A., Devol, A. H., Deutsch, C., 2007. New Developments in the Marine Nitrogen Cycle. Chem. Rev., 107(2), 577–589.

Carslaw, H. S., Jaeger, J. C., 1959. Conduction of Heat in Solids. Oxford University Press, London, UK, Second Edition, 92–132.

Crispi, G., Pacciaroni, M., Viezzoli, D., 2006. Simulating biomass assimilation in a Mediterranean ecosystem model using SOFA: setup and identical twin experiments. Ocean Sci., 2(2), 123–136.

Crispi, G., 2022. Geochimica del carbonio disciolto in ecosistemi pelagici e bentonici. DOI 10.13120/A55052D6-787F-4AA3-9407-2FAB53703C46, 2020/70 Sez OCE 19 EXO, OGS, Trieste, IT, pp. 56.

Gaidos, E., Dubuc, T., Dunford, M., McAndrew, P., Padilla-Gamiño, J., Studer, B., Weersing, K., Stanley, S., 2007. The Precambrian emergence of animal life: a geobiological perspective. Geobiology, 5(4), 351–373.

Galloway, J. N., Dentener, F. J., Capone, D. G., Boyer, E. W., Howarth, R. W., Seitzinger, S. P., Asner, G. P., Cleveland, C. C., Green, P. A., Holland, E. A., Karl, D. M., Michaels, A. F., Porter, J. H., Townsend, A. R., Vörösmarty, C. J., 2004. Nitrogen cycles: past, present, and future. Biogeochemistry, 70(2), 153–226.

Ebenhöh, W., Kohlmeier, C., Radford, P. J., 1995. The benthic biological submodel in the European Regional Seas Ecosystem Model. Neth. J. Sea Res., 33(3/4), 423–452.

Herndl, G. J., Peduzzi, P., Fanuko, N., 1989. Benthic community metabolism and microbial dynamics in the Gulf of Trieste (Northern Adriatic Sea). Mar. Ecol. Prog. Ser., 53, 169–178.

Luff, R., Moll, A., 2004. Seasonal dynamics of the North Sea sediments using a three-dimensional coupled sediment–water model system. Cont. Shelf Res., 24(10), 1099–1127.

Peng, T.-H., Takahashi, T., Broecker, W. S., Olafsson, J., 1987. Seasonal variability of carbon dioxide, nutrients and oxygen in the northern North Atlantic surface water: observations and a model. Tellus, 39(B5), 439–458.

Ruardij, P., Van Raaphorst, W., 1995. Benthic nutrient regeneration in the ERSEM ecosystem model of the North Sea. Neth. J. Sea Res., 33(3/4), 453–483.

Van Cappellen, P., 2004. Biomineralization and Global Biogeochemical Cycles. Rev. Mineral. Geochem., 54(1), 357–381.

Vichi, M., Oddo, P., Zavatarelli, M., Coluccelli, A., Coppini, G., Celio, M., Fonda Umani, S., Pinardi, N., 2003. Calibration and validation of a one-dimensional complex

marine biogeochemical flux model in different areas of the northern Adriatic shelf. Ann. Geophys., 21(1), 413–436.

Wanninkhof, R., 1992. Relationship Between Wind Speed and Gas Exchange Over the Ocean. J. Geophys. Res., 97(C5), 7373–7382.

Keywords: Carbon Dioxide, Benthos, Diffusion Processes, Marine Environment

Abstract: The dynamics of the aquatic ecosystem requires a thorough knowledge of the chemical and physical parameters in both the water column and the sediment. The constitutive equations of the former subsystem solve diffusion and transport processes in three-dimensional domains; the latter is described by one-dimensional and nonlinear differential equations whose solution strongly depends on slower diffusion parameters.

An evolution method, CO_2-Geo, which minimises the squared deviation between the exact evolution and the consistent prediction with the transformation method, is developed and verified to estimate the single-layer evolution and the three-layer sediment description based on the diffusion parameters in the porewater. The method is generic and is extended here to the trophic behaviour of carbon dioxide and methane.

Geochemistry of dissolved carbon in pelagic and benthic ecosystems
Crispi
57 pp. June 2023